ChemComm

COMMUNICATION

Synthesis of Pt–Ni/graphene *via in situ* reduction and its enhanced catalyst activity for methanol oxidation†

Lihong Li, Yuen Wu, Jun Lu, Caiyun Nan and Yadong Li*

A simple *in situ* reduction approach was used to obtain Pt₃Ni/reduced graphene oxide (rGO) with dominant {111} facets. The catalytic activity of Pt–Ni/rGO toward methanol electro-oxidation was studied by performing cyclic voltammetry. The Pt₃Ni/rGO nanocatalysts exhibited improved catalytic activity and durability.

Noble nanoparticles (NPs, *i.e.* Pt,[1] Pd,[2] *etc.*) with well-defined sizes, compositions and facets have been widely used as catalysts in many applications, such as fuel cells and so on.[3–12] To improve the atomic efficiency and sustainability, researchers have studied the Pt-based bimetallic nanostructures, in which Pt is partially replaced by cheap 3d-transition metals (*i.e.* Fe, Co, Ni, Cu, *etc.*) as promising substitutions.[13–16] Furthermore, previous studies indicated that a 9-fold enhancement of the area-specific oxygen reduction activity was achieved by changing from the {100} to the {111} Pt₃Ni crystal surface. Meanwhile, the oxygen reduction activity on the {111} Pt₃Ni surface is 10-fold higher than that on the {111} Pt surface, because the shift of the d-band centre increases with the removal rate of adsorbed O and OH species.[13] Therefore, by using Pt–Ni nanoparticles with the dominant {111} surface as a catalyst, it is expected that the catalytic performance could be optimized in the fuel cell reactions.

As we all know the activity and durability of carbon-supported NPs in fuel cell reactions are of great concern to both industry and academia.[17] Recently, graphene (or reduced oxide graphene, rGO) has attracted attention as a unique 2D material with low cost, high surface area, good electrical conductivity and high mechanical strength, which can not only maximize the availability of a nanosized electrocatalyst surface area for electron transfer, but can also provide enhanced mass transport of reactants to the electrocatalyst.[18–20] Thus, intensive effort has focused on using graphene as a catalyst support. It was reported

that the graphene supported alloy nanoparticles were commonly obtained by adding graphene during the reducing metal precursors reaction or mixing the NPs with graphene.[21–24] However, these studies often needed to maximize the contact and interaction between graphene and NPs, and the process consisted of multiple steps, such as pre-modification of graphene or further treatment of the as-prepared NPs/graphene.[13] Therefore, some studies focused on the *in situ* growth method, by which the catalyst nanoparticles could directly grow on the graphene oxide surface, to form close contact.[25] But the nanoparticles prepared by these methods lack the desired size and morphology. Therefore, it is interesting, *via* an *in situ* growth method, to load Pt–Ni nanoparticles with the (111) dominant surface on graphene.

Herein, we report a simple one-pot approach to obtain reduced graphene oxide supported truncated-octahedral Pt–Ni catalysts with a series of Pt–Ni ratio (1 : 0, 3 : 1, 3 : 2, 1 : 1), which dominantly expose {111} facets, *via* the reduction of graphene oxide (GO) and by varying the corresponding amount of Pt and Ni precursors. In our synthetic method, ascorbic acid (VC) was believed to act as a reductant and affected the reaction kinetics. The as-synthesized Pt₃Ni/rGO NPs, which showed satisfactory stability, were evaluated as the most active catalysts for methanol oxidation of the Pt–Ni/rGO and the commercial Pt/C.

Fig. 1 shows the TEM images of Pt–Ni/rGO nanocatalysts, which exhibit remarkable monodispersity and homogeneity. They are well dispersed on the graphene surface. The average size of nanoparticles was approximately 11 nm. In our synthetic method, benzyl alcohol was used as a solvent and reductant, and VC was believed to act as an effective reductant and affect the reaction kinetics, according to the notation.[26] In a control experiment, the irregular Pt–Ni NPs on rGO were observed without the addition of VC. Meanwhile, the substitution of VC with benzoic acid would result in large NPs (see Fig. S1, ESI†). The crystalline structures of the Pt–Ni/rGO samples were confirmed by XRD measurements (Fig. S2, ESI†). It is shown that, after reaction, the interplanar distance of the rGO is decreased to 3.73 Å (23.8°) from 8.60 Å (10.3°) for the original GO, due to the elimination of the oxygen-containing groups on

Department of Chemistry, Tsinghua University, Beijing 100084, China.
E-mail: ydli@mail.tsinghua.edu.cn; Fax: +86-10-62792798; Tel: +86-10-72772350
† Electronic supplementary information (ESI) available: Detailed experimental procedures, further TEM and SEM images, EDS, XRD patterns, XPS patterns and different catalysts' voltammetric responses. See DOI: 10.1039/c3cc44514c
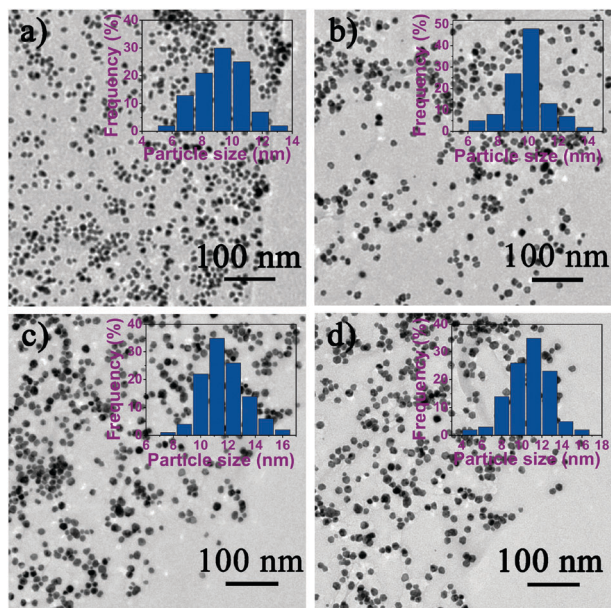
Fig. 1 Pt–Ni/rGO nanocatalysts synthesized at Pt^{2+}/Ni^{2+} molar ratios of (a) 1 : 0, (b) 3 : 1, (d) 3 : 2, and (f) 1 : 1. The insets show the size distribution of the prepared Pt–Ni on rGO synthesized at different Pt/Ni molar ratios.

Fig. 2 (a) Schematic illustration of the controlled synthesis and (b) the HRTEM of Pt_3Ni/rGO nanocatalysts, (c) HAADF-STEM images of Pt_3Ni/rGO truncated octahedrons, corresponding element maps showing the distribution of Pt (yellow) and Ni (red).

the graphene sheets, as reported in ref. 21 and 27. Exactly as shown in Fig. S1c (ESI†), the peaks of Pt/rGO at 39.8° and 46.4° are characteristic of face-centered-cubic crystalline Pt, corresponding to the planes (111) and (200) (JCPDS 04-0802). It should be noted that the peaks continuously shift from the Pt standard peaks to Ni standard ones when the content of Ni increases (Fig. 1d–f). The atomic ratios between Pt and Ni were further verified using Energy-dispersive X-ray spectroscopy (EDX), suggesting that the composition of the product could be effectively controlled by the ratios of the Pt and Ni precursors (Table S1, ESI†).

To further reveal the formation and structure of Pt–Ni/rGO, the high-resolution TEM (HRTEM) measurement of Pt_3Ni/rGO was also done. Fig. 2a shows a typical schematic illustration of controlled synthesis of Pt_3Ni/rGO nanocatalysts. The HRTEM image in Fig. 2b clearly shows that the lattice spacing of Pt_3Ni is 0.224 nm, which agrees with the d-spacing calculation from the XRD pattern (Table S1, ESI†). This value is slightly smaller than that of the (111) plane of Pt (0.226 nm) due to the contraction of the lattice upon substitution of Pt with Ni atoms. The corresponding elemental maps obtained from high-angle annular dark-field scanning transmission electron microscopy (HAADF-STEM) show that both Pt and Ni are distributed throughout the individual truncated octahedral Pt_3Ni nanocrystals with the dominant face of the (111) plane.

To elucidate the reduction process of rGO, high resolution scans of C 1s peaks in the XPS spectra of GO and rGO are performed. Compared with GO, the peaks in the XPS pattern of rGO at 287 eV dramatically decreased in size, and only a peak with a small tail at 285 eV existed, as shown in Fig. S3, ESI.† The results revealed that, after reduction, C–O, C=O, and O–C=O groups are significantly reduced and the C–C bonds became dominant. The FTIR patterns of GO, rGO, Pt/rGO and Pt_3Ni/rGO
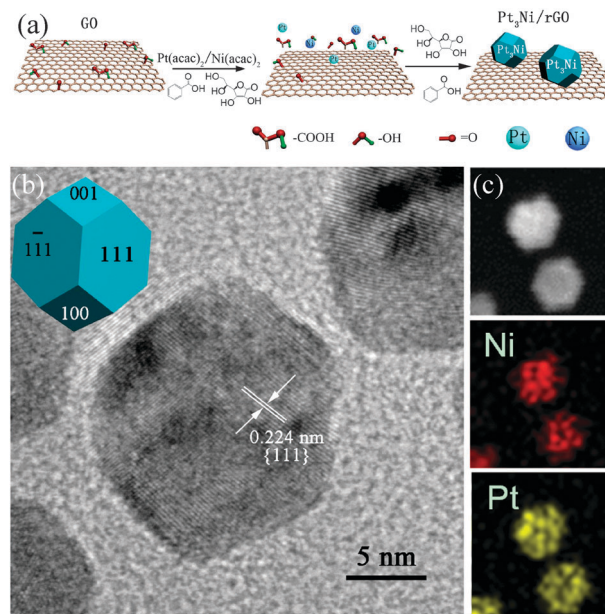
were in agreement with the results, also evidencing that the oxidizing groups were efficiently removed from rGO, Pt/rGO and Pt_3Ni/rGO (Fig. S4, ESI†).

Next we tested our as-synthesized catalysts in the electrical catalytic reaction and compared the results with that of the as-prepared Pt–Ni/active carbon (ESI†) and commercial Pt/C. Fig. 3, Fig. S5 and Table S2 (ESI†) detail the cyclic voltammograms (CVs) normalized to the electrochemical surface area (ECSA) of the different catalysts for methanol oxidation in the electrolytes containing 0.1 M $HClO_4$ + 1 M MeOH. Results clearly show that the forward peak current densities (J_f) are in the order of Pt_3Ni/rGO > Pt_3Ni_2/rGO > $PtNi/rGO$ > $Pt_3Ni/active$ carbon > Pt/rGO > Pt/active carbon > commercial Pt/C, suggesting that
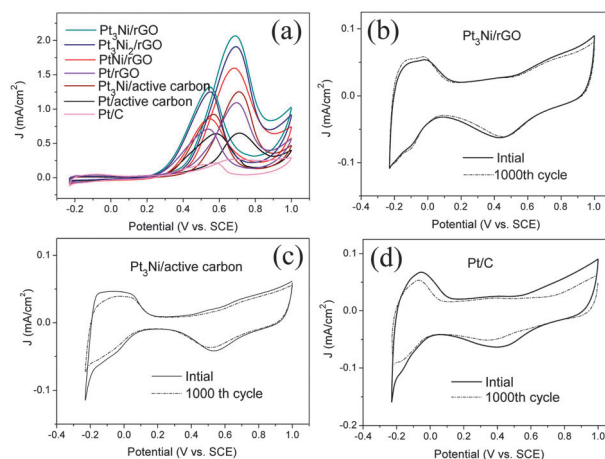

Fig. 3 (a) Cyclic voltammograms of methanol oxidation on different catalysts in 0.1 M $HClO_4$ + 1 M MeOH (scan rate: 50 mV s^{-1}). Cyclic voltammograms of (b) Pt_3Ni/rGO NPs, (c) $Pt_3Ni/active$ carbon, and (d) commercial Pt/C recorded in 0.1 M $HClO_4$ with a scan rate of 50 mV s^{-1}.

graphene can effectively increase the activity of the Pt based catalysts, which may be due to the p-electron polarization from graphene to the Pt based alloy (*via* a possible coordination bonding).[24] The Pt₃Ni/rGO shows superior catalytic activity. The Ni content-dependent catalytic characteristics of the Pt–Ni/rGO nanocatalysts for methanol oxidation can be understood based on the modification of the electronic properties of Pt by Ni in the catalysts, which can be further illustrated from the study of XPS patterns (see Fig. S6, ESI†). It is shown that Pt appears to exist in various states: for dominant Pt^0, a small amount of PtO and $Pt(OH)_2$, and Ni for Ni^0, $Ni(OH)_2$ and NOOH. The existence of noncrystalline oxygen species on the surface of the catalysts renders some favourable properties, such as proton and electronic conductivity, and protection of the catalyst against corrosion during methanol oxidation.[28] Furthermore, Ni can modify the electronic structure of Pt due to the charge transfer from Ni to Pt, leading to a lower density of states at the Fermi level, and reduce the Pt–CO band energy and weaken the CO adsorption on Pt–Ni alloys.[29] It is noteworthy that a further increase in the content of Ni (from Pt : Ni = 3 : 1 to 3 : 2 and 1 : 1) could not result in a continual superior activity of methanol electro-oxidation, because fewer metallic Pt atoms are available on the catalyst surface for methanol chemisorption.

Durability is one of the critical factors for a practical catalyst. To evaluate the stability, the cyclic voltammograms (CVs) of the Pt₃Ni/rGO, Pt₃Ni/active carbon and commercial Pt/C catalysts were carried out in 0.1 mol L^{-1} HClO₄ solution (Fig. 3b–d), respectively. The potential range was set to −0.23–1.0 V *vs.* SCE, and the scan rate was 50 mV s^{-1}. It is observed that the electrochemical surface area (ECSA) of Pt₃Ni/active carbon and commercial Pt/C, respectively, drops to almost 75% and 70% of their initial surface area after a durability test of 1000 cycles. Strikingly, the Pt₃Ni/rGO shows almost no recordable loss of electrochemical surface area even after 1000 cycles. This is a strong evidence to support the better stability of Pt₃Ni/rGO than Pt₃Ni/active carbon and the commercial Pt/C. This can also be confirmed by the TEM observations treaded before and after 1000 cycles of the durability test. After 1000 cycles, the size and morphology of Pt₃Ni of Pt₃Ni/rGO remained nearly the same, but serious aggregation could be found for both Pt₃Ni/active carbon and the commercial Pt/C (Fig. S7, ESI†). Based on the above results, we could easily draw a hypothesis that close contact between graphene and Pt₃Ni effectively prevented Pt₃Ni from segregation. Moreover, the p-electron polarization from graphene to Pt₃Ni, together with the modification of Ni, would guarantee the excellent activity even after 1000 cycles.

In summary, a simple one-pot approach was used to obtain reduced graphene oxide (rGO) supported truncated-octahedral Pt–Ni catalysts with a series of Pt–Ni ratio (1 : 0, 3 : 1, 3 : 2, 1 : 1). In this *in situ* reduction process of graphene oxide (GO), the composition of Pt–Ni alloy which dominantly exposes {111} facets could be carefully controlled by simply varying the corresponding amount of Pt and Ni precursors. It is confirmed that benzyl alcohol was used as a solvent and reductant, and VC was believed to act as a co-reductant and affect the reaction kinetics. The Pt₃Ni/rGO NPs exhibited superior catalytic activity and durability for methanol oxidation compared to the other Pt–Ni/rGO and the commercial Pt/C.

Notes and references

1 C. Zhu, S. Guo and S. Dong, *Adv. Mater.*, 2012, **24**, 2326.
2 T. Kijima, T. Yoshimura, M. Uota, T. Ikeda, D. Fujikawa, S. Mouri and S. Uoyama, *Angew. Chem., Int. Ed.*, 2004, **43**, 228.
3 A. D. Smeltz, W. N. Delgass and F. H. Ribeiro, *Langmuir*, 2010, **26**, 16578.
4 S. T. Christensen, J. W. Elam, F. A. Rabuffetti, Q. Ma, S. J. Weigand, B. Lee, S. Seifert, P. C. Stair, K. R. Poeppelmeier, M. C. Hersam and M. J. Bedzyk, *Small*, 2009, **5**, 750.
5 Y. Wu, S. Cai, D. Wang, W. He and Y. Li, *J. Am. Chem. Soc.*, 2012, **134**, 8975.
6 D. S. Wang, Q. Peng and Y. D. Li, *Nano Res.*, 2010, **3**, 574.
7 S. Ye and H. Kita, *J. Electroanal. Chem.*, 1993, **346**, 489.
8 Y. Xu, W. A. Shelton and W. F. Schneider, *J. Phys. Chem. A*, 2006, **110**, 5839.
9 M. C. Wheeler, R. E. Cavicchi and S. Semancik, *J. Phys. Chem. C*, 2007, **111**, 3328.
10 G. A. Somorjai, H. Frei and J. Y. Park, *J. Am. Chem. Soc.*, 2009, **131**, 16589.
11 S. Schäfer, S. A. Wyrzgol, R. Caterino, A. Jentys, S. J. Schoell, M. Hävecker, A. Knop-Gericke, J. A. Lercher, I. D. Sharp and M. Stutzmann, *J. Am. Chem. Soc.*, 2012, **134**, 12528.
12 I. Lee, Z. Ma, S. Kaneko and F. Zaera, *J. Am. Chem. Soc.*, 2008, **130**, 14597.
13 V. R. Stamenkovic, B. Fowler, B. S. Mun, G. Wang, P. N. Ross, C. A. Lucas and N. M. Marković, *Science*, 2007, **315**, 493.
14 J. Wu, J. Zhang, Z. Peng, S. Yang, F. T. Wagner and H. Yang, *J. Am. Chem. Soc.*, 2010, **132**, 4984.
15 T. Ohashi, W. Sugimoto and Y. Takasu, *Diamond Relat. Mater.*, 2011, **20**, 1165.
16 X. F. Yu, D. S. Wang, Q. Peng and Y. D. Li, *Chem. Commun.*, 2011, **47**, 8094.
17 Y. Shao, J. Liu, Y. Wang and Y. Lin, *J. Mater. Chem.*, 2009, **19**, 46.
18 A. K. Geim and K. S. Novoselov, *Nat. Mater.*, 2007, **6**, 183.
19 X. Huang, S. Li, Y. Huang, S. Wu, X. Zhou, S. Li, C. L. Gan, F. Boey, C. A. Mirkin and H. Zhang, *Nat. Commun.*, 2011, **2**, 292.
20 X. Huang, X. Qi, F. Boey and H. Zhang, *Chem. Soc. Rev.*, 2012, **41**, 666.
21 C. Hu, H. Cheng, Y. Zhao, Y. Hu, Y. Liu, L. Dai and L. Qu, *Adv. Mater.*, 2012, **24**, 5493.
22 Y. Li, Y. Li, E. Zhu, T. McLouth, C.-Y. Chiu, X. Huang and Y. Huang, *J. Am. Chem. Soc.*, 2012, **134**, 12326.
23 X. Huang, S. Li, S. Wu, Y. Huang, F. Boey, C. L. Gan and H. Zhang, *Adv. Mater.*, 2012, **24**, 979.
24 S. Guo and S. Sun, *J. Am. Chem. Soc.*, 2012, **134**, 2492.
25 Y. Hu, P. Wu, Y. Yin, H. Zhang and C. Cai, *Appl. Catal., B*, 2012, **111–112**, 208.
26 A. N. Wang, Q. Peng and Y. D. Li, *Chem. Mater.*, 2011, **23**, 3217.
27 S. Pei, J. Zhao, J. Du, W. Ren and H. M. Cheng, *Carbon*, 2010, **48**, 4466.
28 A. Kowal, S. N. Port and R. J. Nichols, *Catal. Today*, 1997, **38**, 483.
29 Q. Jiang, L. Jiang, H. Hou, J. Qi, S. Wang and G. Sun, *J. Phys. Chem. C*, 2010, **114**, 19714.